An Efficient and Accurate Implementation of Centroid Molecular Dynamics Using a Gaussian Approximation†

Being J. Ka and Gregory A. Voth*

Center for Biophysical Modeling and Simulation and Department of Chemistry, University of Utah, Salt Lake City, Utah 84112-0850

Received: July 16, 2005; In Final Form: September 18, 2005

An approximate method for Centroid Molecular Dynamics (CMD) is presented which uses a Gaussian approximation. The resulting method, called Gaussian CMD (GCMD), is 100−1000 times faster than CMD because it replaces explicit path-integral sampling, which is the most time-consuming part of CMD, with a Gaussian averaging, which can be done analytically. Several methods for computing the Gaussian width parameter in the GCMD approach are also presented. This new method is shown to give satisfactory results for the position correlation function in simple one-dimensional systems when CMD itself is consistent with the exact result. The GCMD and CMD results are also compared for the case of 1-dimensional systems coupled to harmonic baths, with good success. GCMD is further compared to CMD with good success for liquid para-hydrogen at two different temperatures, 14 K and 25 K, and for ortho-deuterium at 20.7 K.

I. Introduction

Centroid Molecular Dynamics (CMD) has provided an accurate approximate method to calculate quantum time correlation functions for systems at thermal equilibrium such as those commonly found in the condensed phase. The method was originally proposed by Cao and Voth[1−5] and then rigorously formulated using the quasi-density operator (QDO) concept by Jang and Voth.[6,7] While exact centroid dynamics can also be formulated using the QDO concept,[6] the CMD method itself is not exact because it assumes that the time-dependent QDO, $\hat{\delta}_c(t;x_c,p_c)$, is propagated by virtue of the following approximation[7]

$$\hat{\delta}_c(t;x_c,p_c) \approx \hat{\delta}_c(x_c(t),p_c(t)) \tag{1}$$

where x_c and p_c are the position and momentum path centroid variables, respectively. As a result, the approximate time-dependent QDO in CMD retains its initial form and therefore never has negative regions as does the exact time-dependent QDO in some nonlinear systems. Although it is possible to propagate the QDO in an exact manner, for example, by Numerical Matrix Multiplication (NMM),[8] this becomes essentially impossible as the system goes beyond a few dimensions because the computational effort scales exponentially.

The CMD approximation, on the other hand, has proven to be a powerful approach for obtaining certain quantum dynamical properties of condensed phase systems. Examples of this include proton solvation and transport,[9,10] liquid para-hydrogen,[11−17] liquid nonsuperfluid He,[4,18] Vibrational Energy Relaxation (VER) rate constants,[19−22] vibrational spectroscopy,[23,24] and quantum activated rate constants.[25−27] CMD, of course, has its limitations. The method is intrinsically an approximation most well-suited for condensed phase systems. Such systems usually exhibit fairly rapid regression to equilibrium when evolving from an initially perturbed state and are therefore characterized by fairly strong dissipation. However, an important property of CMD is that the system decays to the correct equilibrium state—a property not shared by many approximate methods.

Sometimes CMD calculations are demanding if the system is too large or when it is coupled to another expensive calculation, for example, an ab initio calculation.[28] CMD calculations in general take longer than classical MD calculations by a factor related to the number of path integral discretizations times the required sampling to calculate the centroid force. In many cases, this can amount to simulations 100−1000 times more expensive than classical MD. It is therefore desirable to have a more efficient approach for CMD simulations, and the present work is devoted to this goal. In particular, we introduce a new CMD algorithm that uses a Gaussian representation of the QDO. A different approach for efficient CMD is to use force-match to predetermine an effective pairwise centroid force between particles.[29]

The present paper includes a formal derivation of several approximations in section II and then compares these methods for typical model systems in section III. Section IV contains concluding remarks.

II. Theory

A. Exact Initial QDO and the CMD Approximation. The diagonal element of the exact initial QDO, eq 17 of ref 6, is given by

$$\langle x|\hat{\delta}_c(x_c)|x\rangle = \frac{\langle x|\hat{\varphi}(x_c)|x\rangle}{\rho_c(x_c)} = \frac{1}{\rho_c(x_c)}\sqrt{\frac{2\pi\hbar^2\beta}{m}}\lim_{P\to\infty}\left(\frac{mP}{2\pi\hbar^2\beta}\right)^{P/2}\int dx_2 \ldots \int dx_P \delta(x_c - x_0) \times \exp\left\{-\frac{mP}{2\hbar^2\beta}[(x-x_2)^2 + \cdots + (x_P - x)^2] - \frac{\beta}{P}[V(x) + V(x_2) + \cdots + V(x_P)]\right\} \tag{2}$$

† Part of the special issue "Jack Simons Festschrift".

* Corresponding author phone: (801)581-7272; fax: (801)581-4353 or 8433; e-mail: voth@chem.utah.edu.

10.1021/jp053919j CCC: $30.25
Published on Web 10/25/2005

where the position centroid distribution is given by

$$\rho_c(x_c) \equiv \sqrt{\frac{2\pi\hbar^2\beta}{m}}\int_{x(0)=x(\beta\hbar)} Dx(\tau)\delta(x_c - x_0)e^{-S[x(\tau)]/\hbar} = \sqrt{\frac{2\pi\hbar^2\beta}{m}}\lim_{P\to\infty}\left(\frac{mP}{2\pi\hbar^2\beta}\right)^{P/2}\int dx_1 ... \int dx_P \delta(x_c - x_0) \times \exp\left\{-\frac{mP}{2\hbar^2\beta}[(x_1 - x_2)^2 + \cdots + (x_P - x_1)^2] - \frac{\beta}{P}[V(x_1) + V(x_2) + \cdots + V(x_P)]\right\} \quad (3)$$

and the centroid variable in discretized path integral notation is written as $x_0 = (x_1 + x_2 + \cdots + x_P)/P$. A one-dimensional notation is used throughout this paper, which is readily generalized to an arbitrary number of particles in three dimensions.

The exact time-dependent QDO is defined as

$$\hat{\delta}_c(t;x_c,p_c) \equiv e^{-i\hat{H}t/\hbar}\hat{\delta}_c(x_c,p_c)e^{i\hat{H}t/\hbar} \quad (4)$$

which is approximated by

$$\hat{\delta}_c(t;x_c,p_c) \approx \hat{\delta}_c(x_c(t),p_c(t)) \quad (5)$$

in the CMD formalism and thus leads to the practical implementation of centroid dynamics. As stated earlier, an important goal is to find more efficient methods for CMD simulations in realistic condensed phase systems. Equation 5 defines time-dependent CMD variables and their time correlation functions (TCFs) as, respectively

$$B_c(t) = Tr[\hat{\delta}_c(x_c(t),p_c(t))\hat{B}] \quad (6)$$

$$C_{AB}^{\mathrm{CMD}}(t) \equiv \frac{1}{Z}\int\int\frac{dx_c dp_c}{2\pi\hbar}\rho_c(x_c,p_c)A_c B_c(t) \quad (7)$$

with the CMD equations of motion for $x_c(t)$ and $p_c(t)$ given by

$$\frac{dx_c(t)}{dt} = \frac{p_c(t)}{m} \quad (8)$$

$$\frac{dp_c(t)}{dt} = F_c(t) \quad (9)$$

B. Gaussian Approximation. The QDO at higher temperature can be shown to assume a Gaussian form.[6] It is therefore natural to develop a Gaussian approximation which, in turn, makes the CMD algorithm much more efficient. As the QDO is normalized to unity, the Gaussian QDO (GQDO) at each centroid position is defined by a single parameter, its width. To determine the best expression for the width of the GQDO, one looks to the exact expression for the QDO in the limit of a harmonic potential. If a potential is harmonic, i.e., given by

$$V(x) = \frac{m\Omega^2}{2}x^2 \quad (10)$$

its QDO element is given by

$$\langle x'|\hat{\delta}_c(x_c,p_c)|x\rangle_\Omega = \sqrt{\frac{m\Omega}{\pi\hbar\alpha}}\exp\left[-\frac{m\Omega\alpha}{4\hbar}(x' - x)^2 + \frac{i}{\hbar}p_c(x' - x) - \frac{m\Omega}{\hbar\alpha}\left(\frac{x' + x}{2} - x_c\right)^2\right] \quad (11)$$

where

$$\alpha \equiv \coth(\Omega\hbar\beta/2) - (2/\Omega\hbar\beta) \quad (12)$$

If the potential is not harmonic, eq 11 can still be approximately applied for a general potential. Below two different approximations will be given for the approximate widths of the Gaussian QDO.

C. Choices for the Gaussian Width. *1. Free Particle Width: GCMD-0.* The expression for the QDO in a free particle potential (GQDO-0) is obtained in the limiting case of eq 11 as $\Omega \to 0$, i.e.

$$\langle x'|\hat{\delta}_G(x_c,p_c)|x\rangle = \sqrt{\frac{\gamma_G(\beta)}{\pi}}\exp\left[-\gamma_G(\beta)\left(\frac{x' + x}{2} - x_c\right)^2 + \frac{i}{\hbar}p_c(x' - x)\right] \quad (13)$$

where $\gamma_G(\beta) \equiv 6m/(\hbar^2\beta)$. This GQDO-0 expression gives some degree of quantum behavior for the system. As $\gamma_G(\beta) \to \infty$ at a very high temperature (or with a very heavy particle), the GQDO becomes a delta function centered at the centroid position, so the particle thus behaves in a classical manner.

2. Local Harmonic Approximation: GCMD-I. In the limit of low temperature, the exact QDO becomes more position-dependent, especially if the potential is anharmonic. The free-particle (or a fixed width) approximation of the GQDO (GQDO-0) therefore seems less realistic, and a more accurate approximation for the GQDO is required. Again, there is obviously no analytical expression for the exact QDO, so a centroid-position-dependence of the GQDO can be inferred from a case in which an analytic expression for the QDO is known. One such case is the harmonic potential.

Because an analytical expression for the QDO is available in the form of eq 11, one can introduce a local harmonic approximation for a general potential, $V(x)$. In the local harmonic approximation, a general potential in the neighborhood (x) around each centroid point, x_c, is approximated as a Taylor expansion up to a quadratic term by

$$V(x) \approx V(x_c) + \frac{\partial V(x)}{\partial x}|_{x=x_c}(x - x_c) + \frac{1}{2}m[\Omega_G(x_c)(x - x_c)]^2 \quad (14)$$

where $\Omega_G(x_c)$, which replaces Ω of eq 11 in the local harmonic approximation, is defined as

$$\Omega \to \Omega_G(x_c) \equiv \sqrt{\frac{1}{m}\frac{\partial^2 V(x)}{\partial x^2}|_{x=x_c}} \quad (15)$$

As a result, the GQDO becomes

$$\langle x'|\hat{\delta}_G(x_c)|x\rangle = \sqrt{\frac{\gamma_G(x_c;\beta)}{\pi}}\exp\left[-\frac{\gamma_G(x_c;\beta)\alpha^2}{4}(x' - x)^2 + \frac{i}{\hbar}p_c(x' - x) - \gamma_G(x_c;\beta)\left(\frac{x' + x}{2} - x_c\right)^2\right] \quad (16)$$

where

$$\gamma_G(x_c;\beta) \equiv \frac{m\Omega_G(x_c)}{\hbar\alpha_G(x_c;\beta)},\ \alpha_G(x_c;\beta) \equiv \coth\left(\frac{\Omega_G(x_c)\hbar\beta}{2}\right) - \frac{2}{\Omega_G(x_c)\hbar\beta} \quad (17)$$

The value of $\Omega_G(x_c)$ above becomes an imaginary number when the local curvature of potential is negative, which can limit the application of the Gaussian approximation for the QDO. This problem can be avoided, however, by using the QDO of

the free particle in the region that the curvature of potential goes negative, i.e.

$$\gamma_G(x_c;\beta) \equiv \frac{m\Omega_G(x_c)}{\hbar\alpha_G(x_c;\beta)} \quad \text{for } V''(x_c) > 0 \tag{18}$$

$$\equiv \frac{6m}{\hbar^2\beta} \quad \text{for } V''(x_c) \le 0$$

because

$$\alpha_G \to 0 \text{ and } \alpha_G/\Omega_G \to \beta\hbar/6 \text{ as } \Omega_G \to 0$$

D. Gaussian Centroid Force. Once a GQDO is given, the Gaussian centroid force, F_G, is required to propagate the centroid variables. This force is given by

$$F_G(x_c) = Tr[\hat{\delta}_G\hat{F}] = \int dx\, f(x)\cdot\sqrt{\frac{\gamma_G}{\pi}}e^{-\gamma_G(x-x_c)^2} \tag{19}$$

For any force which is expanded in a polynomial form

$$f(x) = -\frac{\partial V(x)}{\partial x} = \sum_n b_n x^n \tag{20}$$

the Gaussian centroid force has the following form

$$F_G(x_c) = \sqrt{\frac{\gamma_G}{\pi}}\sum_n b_n \sum_{k=0}^{n}\binom{n}{k}\frac{\Gamma((n-k+1)/2)}{\gamma_G^{(n-k+1)/2}}x_c^{\,k}, \quad k = 0,1,2,\ldots,n \tag{21}$$

where Γ is the gamma function and $\binom{n}{k}$ is $n!/(k!(n-k)!)$ for even $n-k$ or zero for odd $n-k$.

Other forces, which cannot be expanded in polynomial forms, are still expandable in Gaussian functions, i.e.

$$f(x) = -\frac{\partial V(x)}{\partial x} = \sum_n [a_n + b_n e^{-c_n(x-x_n)^2}] \tag{22}$$

and their corresponding Gaussian centroid forces are given by

$$F_G(x_c) = \sum_n \left[a_n + b_n\sqrt{\frac{\gamma_G}{\gamma_G + c_n}}e^{-\gamma_G c_n(x_c-x_n)^2}\right] \tag{23}$$

The Gaussian centroid force in many-particle systems can be defined in a similar way, but this involves additional assumptions. This approach is discussed in the Appendix.

E. Propagation of Centroid Variables and Quantum Time Correlation Functions. Once initial centroid points, (x_c,p_c) are sampled according to the centroid distribution function, eq 24, where the sampling of p_c is a just Gaussian sampling

$$\rho_c(r_c,p_c) = e^{-\beta p_c^2/2m}\rho_c(r_c) \tag{24}$$

those centroid variables are propagated by eqs 25 and 26 under the Gaussian centroid force of section II.D such that

$$\frac{dx_c(t)}{dt} = \frac{p_c(t)}{m} \tag{25}$$

$$\frac{dp_c(t)}{dt} = F_G(t) \tag{26}$$

which gives the time-dependent centroid variables, $x_c(t)$ and $p_c(t)$. The time-dependent velocity centroid variable, $v_c(t)$ then gives the centroid velocity correlation function, $C_{vv}^{cen}(t)$, as

$$C_{vv}^{cen}(t) = \frac{1}{Z}\int\int\frac{dx_c dp_c}{2\pi\hbar}\rho_c(x_c,p_c)v_c v_c(t) \tag{27}$$

$$= \frac{1}{N_c}\sum_{i=1}^{N_c}\frac{1}{t_{\max}}\sum_{t_0=0}^{t_{\max}-1} v_{c,i}(t_0)v_{c,i}(t_0+t) \tag{28}$$

where $Z \equiv \int\int dx_c dp_c/(2\pi\hbar)\rho_c(x_c,p_c)$ and N_c is number of sampled centroid points. Equation 28 is a practical form to get eq 27, and averaging over $t_{\max}$ gives more rapid convergence.

The centroid velocity correlation function, $C_{vv}^{cen}(t)$ is used in the following Fourier transform relationship[3]

$$\tilde{C}_{vv}^{qm}(\omega) = \frac{\hbar\beta\omega}{2}\left[\coth\left(\frac{\hbar\beta\omega}{2}\right)+1\right]\tilde{C}_{vv}^{cen}(\omega) \tag{29}$$

to give an approximation to the quantum velocity correlation function, $C_{vv}^{qm}(t)$, which is one of the main goals in this calculation and whose formal expression is given by

$$C_{vv}^{qm}(t) \equiv Tr[e^{-\beta\hat{H}}\hat{v}e^{i\hat{H}t/\hbar}\hat{v}e^{-i\hat{H}t/\hbar}]/Tr[e^{-\beta\hat{H}}] \tag{30}$$

The tilde in eq 29 denotes the Fourier transform, and eqs 28 and 29 are working equations for the calculation of $C_{vv}^{qm}(t)$. In the same way, position autocorrelation functions can be obtained by replacing v with x in eq 27 through eq 30.

III. Examples

A. One-Dimensional Potentials. The models studied here are the same ones that have been studied with CMD and exact methods before.[7] The weak anharmonic potential, eq 31 below, represents many cases where anharmonicity of a system is not large, while the double well potential, eq 32, is a case where the quantum effects such as tunneling become important. The quartic potential, eq 33, is for the test of a large anharmonicity (i.e., there is no quadratic part to this potential). These three potentials are given by

$$V(x) = \frac{1}{2}x^2 + \frac{1}{10}x^3 + \frac{1}{100}x^4 \tag{31}$$

$$V(x) = -\frac{1}{2}x^2 + \frac{1}{10}x^4 \tag{32}$$

$$V(x) = \frac{1}{4}x^4 \tag{33}$$

1. Centroid Distribution. At the initial step of the simulation, the centroid variables x_c,p_c are sampled according to the centroid distribution function, eq 24. Sampling of p_c follows simply a Gaussian distribution, while x_c is sampled by Path Integral Molecular Dynamics (PIMD) with a discretization of $P = 10$ according to eq 3. Also Nosé-Hoover chain dynamics[30] and the VV-3 algorithm developed by Jang and Voth[31] (length of chain = 4 and Nosé masses = 2) were used for sampling of x_c. The initial PIMD ring-polymer was relaxed 1,000,000 steps with a time step of 0.01, and then the centroid positions of every 10,000 steps were collected until the total number of x_c initial conditions reached 10,000.

2. Quantum Position Correlation Function. Once the time-dependent position centroid variable is obtained, it gives the centroid position correlation function, $C_{xx}^{cen}(t)$, through eqs 27−

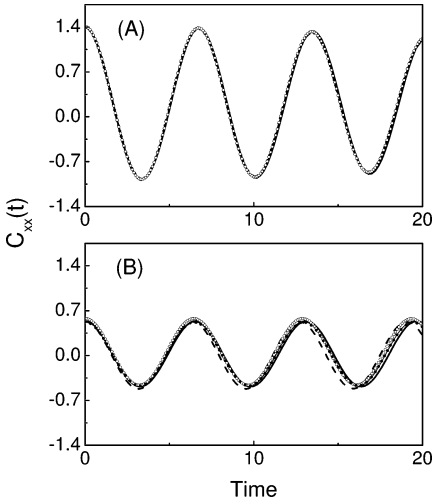

Figure 1. Position time correlation functions for the weak anharmonic of eq 31, at two different temperatures of (A) $\beta = 1$ and (B) $\beta = 8$: exact (thick solid), CMD (dotted), GCMD-0 (open circle), GCMD-I (thin solid), and CCD (dashed).

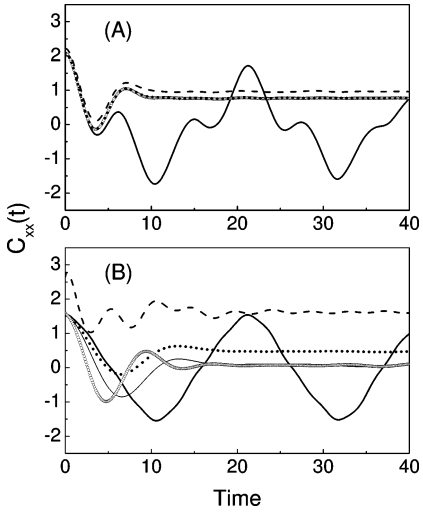

Figure 2. Position time correlation functions for the double well of eq 32, at two different temperatures of (A) $\beta = 1$ and (B) $\beta = 8$: exact (thick solid), CMD (dotted), GCMD-0 (open circle), GCMD-I (thin solid), and CCD (dashed).

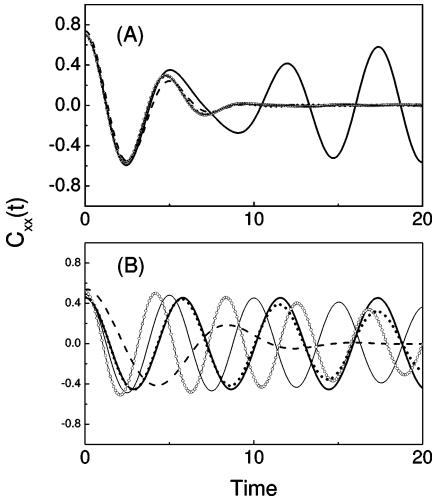

Figure 3. Position time correlation functions for the quartic of eq 33, at two different temperatures of (A) $\beta = 1$ and (B) $\beta = 8$: exact (thick solid), CMD (dotted), GCMD-0 (open circle), GCMD-I (thin solid), and CCD (dashed).

30 but now with x in the place of v. In Figures 1−3, different position correlation functions are compared: exact, CMD, GCMD-0, GCMD-I, and Classical Centroid Dynamics (CCD), for each of the three potentials in eqs 31−33. The CCD method is one in which the centroids are propagated with the classical force, but their initial conditions are sampled from the exact quantum centroid distribution. Exact and CMD data are taken from the paper by Jang and Voth.[7]

Weak Anharmonic Potential [Eq 31]. When the temperature is such that $\beta = 1$, all GCMD, CCD, and CMD results give a good approximation for position correlation functions to the exact one in Figure 1. When $\beta = 8$, all approximate methods deviate from the exact one, although most of the features of the exact result are still captured. CCD and GCMD-0 are somewhat less accurate than GCMD-I or CMD, because the former are not capable of describing the position-dependence of the QDO, which becomes more important as the temperature is lowered.

Double Well Potential [Eq 32]. The double well potential is far from the harmonic case, even for $\beta = 1$, so the results of any approximate method in Figure 2 deviate significantly from the exact correlation function. This behavior arises because the approximate time-dependent position centroid variable, $x_c(t)$, does not follow the exact centroid trajectory after $t \sim 3$ in Figure 3 of ref 32. The CMD assumption in section II.A does not reflect the real behavior of the time-dependent QDO. In reality, the QDO as a function of time can be different even at the same centroid position and momentum, i.e.

$$\hat{\delta}_c(t;x_c,p_c) \neq \hat{\delta}_c(t';x_c,p_c) \text{ for } t \neq t' \tag{34}$$

which is assumed to be an equality in the CMD formalism. This real behavior of the QDO is shown in Figure 1 in the paper by Jang and Voth[6] and the semiclassical centroid dynamics work of Ka and Voth.[32]

In Figure 2 for $\beta = 1$, all GCMD and CMD results are satisfactory up to $t \sim 3$, while the CCD approach shows a larger and earlier deviation from the exact result. When compared to CMD, both GCMD results give a reasonable agreement over the whole range of time. When the temperature is lowered to $\beta = 8$, the GCMD results are in worse agreement with the CMD correlation function and the exact result in comparison to the $\beta = 1$ case. The CCD result deviates seriously, and the GCMD-0 result deviates at early times. The GCMD-I result is better than both CCD and GCMD-0 because it includes a position-sensitive QDO description.

Quartic Potential [Eq 33]. When $\beta = 1$ in Figure 3 for the purely quartic potential, all approximate CMD methods give reasonable correlation functions. The GCMD correlation functions follow the CMD correlation function very well up to $t \sim 5$. When the temperature is lowered to $\beta = 8$, however, only the CMD correlation function exhibits good agreement with the exact correlation function in Figure 3. All other approximate methods fail to follow the exact or CMD correlation beyond $t = 1$, although the GCMD approximations generally have just a phase shift from the CMD results. The CCD result is the worst case in that its dephasing is prominent in comparison to any other method.

Overall these typical 1-dimensional potential examples confirm that CMD works better when anharmonicity is weak or the temperature is high or low but not intermediate. Also they reveal that GCMD is an efficient and satisfactory approximation to CMD in the time range where CMD is consistent with the exact correlation function except for the purely quartic potential

TABLE 1: Frequencies and Coupling Constants for the Harmonic Bath in Section III.B[a]

	c_i/m_i	
ω_i	weak coupling	strong coupling
0.57(0.4)	0.063	0.21
1.13(0.8)	0.102	0.34
1.7(1.2)	0.123	0.41
2.26(1.6)	0.132	0.44
3.11(2.2)	0.132	0.44
3.68(2.6)	0.129	0.43
4.24(3.0)	0.120	0.40
5.09(3.6)	0.108	0.36
5.66(4.0)	0.099	0.33
6.22(4.4)	0.087	0.29

[a] Frequencies in parentheses were used for weak anharmonic or quartic potential cases. All units are in atomic units.

at a temperature of $\beta = 8$. One further expects that (G)CMD will be better in larger systems where dissipation plays an important role. So (G)CMD is tested in the next section for the above systems coupled to a dissipative harmonic bath. GCMD is also applied to many-particle systems in section III.C. Unfortunately, exact calculations for these cases are not available for comparison, so the focus is only on how GCMD works in comparison to CMD.

B. 1D System + Harmonic Baths. Sun and Miller[33] have added 10 harmonic (bath) degrees of freedom to a 1-D system potential in order to investigate the system-bath problem. The same coupling between system and bath modes is used in this work. Specific values of frequencies, $\{\omega_i\}$, and coupling constants, $\{c_i\}$, are listed in Table 1. Two different sets of coupling constants were employed in order to explore how quantum dissipation affects the (G)CMD correlation functions: weak coupling, {0.063, ..., 0.087} and strong coupling, {0.21, ..., 0.29}.

1. Single Well Potential with Weak Anharmonicity + Gaussian Bath. In this case the potential is given by

$$V(x,\{q_i\}) = \frac{1}{2}x^2 + \frac{1}{10}x^3 + \frac{1}{100}x^4 + \sum_{i=1}^{10}\frac{m_i\omega_i^2}{2}\left(q_i - \frac{c_i}{m_i\omega_i^2}x\right)^2 \quad (35)$$

When the coupling is weak (Figure 4A,B), the correlation function of system has almost the same frequency, but the oscillation is somewhat damped in comparison to the case of no coupling. As the coupling becomes strong (Figure 4C,D), the correlation function of the system is modified significantly. Both the frequency and amplitude are changed, and dephasing becomes much more dominant. In both cases, all CMD approximations are in good agreement with one another.

2. Double Well Potential + Gaussian Bath. The potential in this case is given by

$$V(x,\{q_i\}) = -\frac{1}{2}x^2 + \frac{1}{10}x^4 + \sum_{i=1}^{10}\frac{m_i\omega_i^2}{2}\left(q_i - \frac{c_i}{m_i\omega_i^2}x\right)^2 \quad (36)$$

It is shown from comparison of Figures 2 and 5 that the (G)CMD correlation function has more structure when the system is coupled to a bath. Figure 5A,C shows that regardless of the strength of the coupling, if $\beta = 1$ all approximations give a reasonable result. When $\beta = 8$ and the coupling is weak, CCD gives poor agreement with the CMD result, while GCMD captures more of the CMD behavior, with GCMD-I being the best.

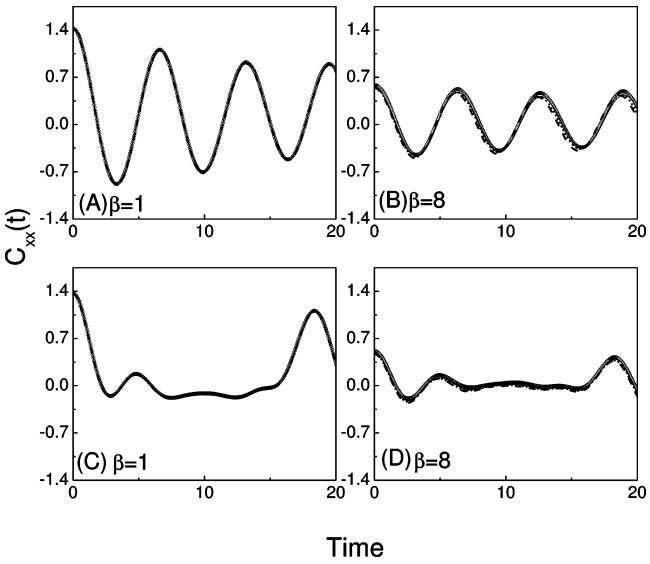

Figure 4. Position time correlation functions for the weak anharmonic potential weakly (A and B) or strongly (C and D) coupled to 10 harmonic bath modes at two different temperatures of $\beta = 1$ (A and C) and $\beta = 8$ (B and D): CMD (dotted), GCMD-0 (open circle), GCMD-I (thin solid), and CCD (dashed).

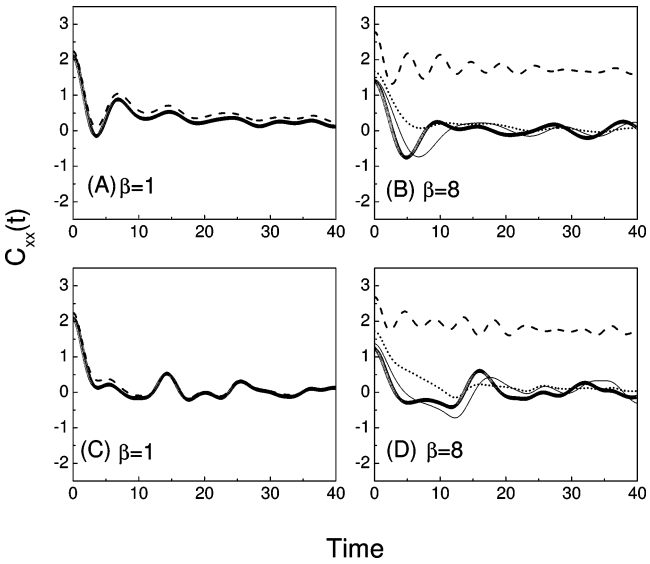

Figure 5. Position time correlation functions for the double well potential weakly (A and B) or strongly (C and D) coupled to 10 harmonic bath modes at two different temperatures of $\beta = 1$ (A and C) and $\beta = 8$ (B and D): CMD (dotted), GCMD-0 (open circle), GCMD-I (thin solid), and CCD (dashed).

3. Quartic Potential + Gaussian Bath. The potential in this case is given by

$$V(x,\{q_i\}) = \frac{1}{4}x^4 + \sum_{i=1}^{10}\frac{m_i\omega_i^2}{2}\left(q_i - \frac{c_i}{m_i\omega_i^2}x\right)^2 \quad (37)$$

From a comparison of Figures 3 and 6, when $\beta = 1$ the correlation functions from (G)CMD show more structure at later times if bath modes are coupled to the system dynamics. It appears that somehow the coupling to the bath may serve to reduce the anomalous dephasing of the CMD result at $\beta = 1$ for this potential as seen in Figure 3. Both GCMD approximations seem to follow the CMD correlation function reasonably well, while CCD remains a poor approximation at the low temperature ($\beta = 8$).

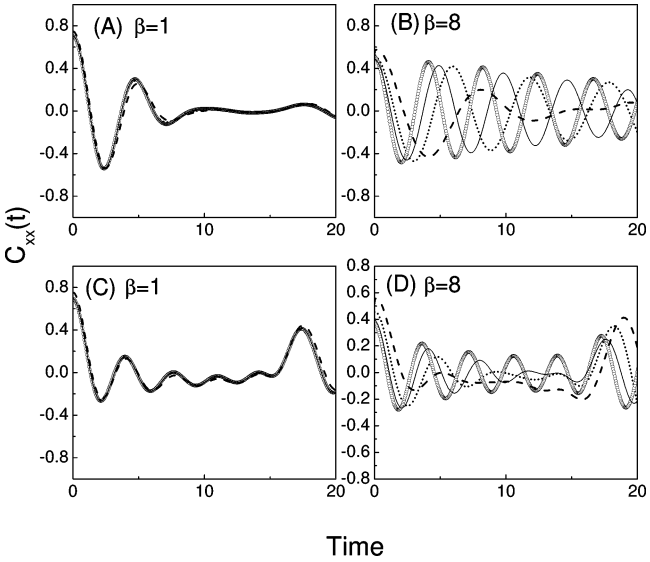

Figure 6. Position time correlation functions for the quartic potential weakly (A and B) or strongly (C and D) coupled to 10 harmonic bath modes at two different temperatures of $\beta = 1$ (A and C) and $\beta = 8$ (B and D): CMD (dotted), GCMD-0 (open circle), GCMD-I (thin solid), and CCD (dashed).

TABLE 2: Parameters for the Silvera−Goldman Potential Function for Ground State H_2-H_2[a]

potential	a	b	c	r_m	C_6	C_8	C_9	C_{10}
$V_{H_2-H_2}$	1.713	1.5671	0.00993	6.50	12.14	215.2	143.1	4813.9

[a] The units for each quantity are atomic units. Taken from Table 1 of ref 36.

C. Many-Particle Systems. *1. Gaussian Fitting of the Silvera−Goldman Potential for Para-H_2.* Hydrogen molecules can be approximated to be in their rotational ground state. This approximation is justified at temperatures below 85 K, the rotational temperature of hydrogen molecule.[11] The interaction between such spherical hydrogen "molecules" is described by the Silvera−Goldman potential,[34] given by

$$V_{SG}(r) = \exp[a - br - cr^2] - \left[\frac{C_6}{r^6} + \frac{C_8}{r^8} - \frac{C_9}{r^9} + \frac{C_{10}}{r^{10}}\right] f_c(r) \tag{38}$$

where

$$f_c(r) = \begin{cases} \exp[-(1.28(r_m/r) - 1)^2], & r < 1.28r_m \\ 1, & r \geq 1.28r_m \end{cases} \tag{39}$$

The parameters of eqs 38 and 39 are found in Table 2. In Appendix A, fitting of the Silvera−Goldman forces by Gaussian functions is presented, which were used in our GCMD simulations.

2. GCMD Simulations. The equilibrium state of liquid para-hydrogen at 25 K (or 14 K) was achieved through relaxation of an initial fcc structure where 500 molecules were packed periodically within an equilateral cubic simulation box. After an initial 10 ps relaxation, 300 4.2 ps runs were carried out with a time step of $dt = 1$ fs, each starting from the final configuration of the last run. Whenever the next run started, velocities of the particles were resampled according to eq 24 to ensure canonical sampling. Data were collected from the final 100 runs, and no data were collected for the first 200 fs of each run. For sampling of para-hydrogen at $T = 25$ K and ortho-deuterium at $T = 20.7$ K, the second set of 100 4.2 ps runs were enough, but para-hydrogen at $T = 14$ K required longer equilibration runs. This is because relaxation from initial lattice structure occurs more slowly at a lower temperature.

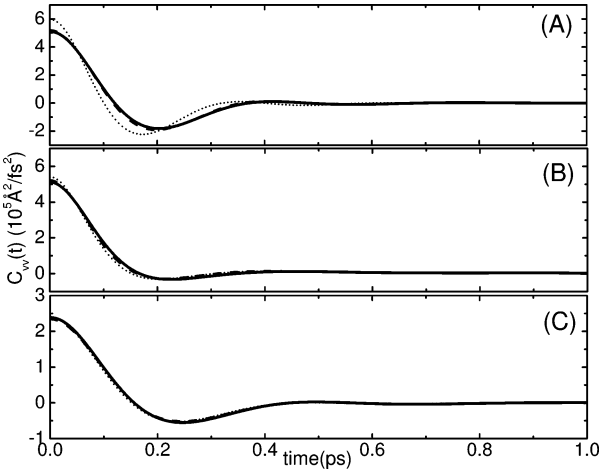

Figure 7. Velocity correlation functions of (A) para-hydrogen at $T = 14$ K, (B) para-hydrogen at $T = 25$ K, and (C) ortho-deuterium at $T = 20.7$ K. The three curves are CMD (thick solid line), GCMD-0 (dotted line), and GCMD-I (dashed line).

TABLE 3: Self-Diffusion Constants for Liquid Para-Hydrogen at 25 K (Å^2/ps)

method	Green-Kubo	density (Å^{-3})
CMD (ref 17)	1.52 ± 0.08	0.0190
GCMD-0	1.46 ± 0.05	0.0190
GCMD-I	1.54 ± 0.07	0.0190
experiment (ref 37)	1.6	

TABLE 4: Self-Diffusion Constants for Liquid Para-Hydrogen at 14 K (Å^2/ps)

method	Green-Kubo	density (Å^{-3})
CMD (ref 17)	0.35 ± 0.05	0.0235
GCMD-0	0.22 ± 0.05	0.0230
GCMD-I	0.32 ± 0.06	0.0230
experiment (ref 37)	0.4	0.0230

3. Velocity Correlation Function and Self-Diffusion Constants. Velocity autocorrelation functions, $C_{vv}(t) = \langle \mathbf{v}_c(0)\mathbf{v}_c(t)\rangle_{\rho_c}$, were calculated from simulation runs for 3 cases and appear in Figure 7 (A−C). In all three figures, there are some relatively small differences between exact CMD and GCMD (−0, or −I). Of the three systems, para-hydrogen at $T = 14$ K is most quantum in nature, and therefore one can see larger differences between GCMD-0 and GCMD-I from Figure 7A. Differences between methods become smaller as the temperature goes higher (Figure 7B) or the mass gets heavier (Figure 7C).

The self-diffusion constants, D, were calculated through the Green-Kubo formula[5,11] where a numerical integration is performed over Figure 7(A−C) such that

$$D = \frac{1}{3}\int_0^\infty dt \langle \mathbf{v}_c(0)\mathbf{v}_c(t)\rangle_{\rho_c} \tag{40}$$

The values for the diffusion constants are listed in Tables 3 −5 for the three systems studied. Para-hydrogen at $T = 25$ K (Table 3) is well described by both forms of GCMD, while at $T = 14$ K (Table 4), the two GCMD approximations give different diffusion constants. Of these choices, GCMD-I seems most reasonable as might be expected since it employs a more physically accurate local quadratic width than the free particle

TABLE 5: Self-Diffusion Constants for Liquid Ortho-Deuterium at 20.7 K (Å²/ps)

method	Green-Kubo	density (Å^{-3})
CMD (ref 17)	0.40 ± 0.06	0.0254
GCMD-0	0.38 ± 0.06	0.0254
GCMD-I	0.41 ± 0.06	0.0254
experiment (ref 38)	0.36	0.0254

width of GCMD-0. This result also implies that a position sensitivity of the QDO at a lower temperature is more important.

For o-deuterium at $T = 20.7$ K (Table 5), there is a less difference between the GCMD results, which may be ascribed to a relatively heavy mass of deuterium in comparison to that of hydrogen, making it more classical. Overall GCMD-I gives very satisfactory diffusion constants for all three cases, which is an encouraging result from this work.

IV. Concluding Remarks

In this paper, a Gaussian-approximation for CMD (GCMD) has been introduced in order to greatly increase the speed and efficiency of CMD calculations. GCMD is clearly a good choice when CMD is expected to give a result consistent with the exact one, for example, condensed phase systems when dissipation from one degree of freedom of interest to other degrees of freedom is prominent. GCMD is very efficient in terms of computational effort, e.g., it requires ~1/100th the CPU time compared to full CMD, and is only 2−3 times slower than conventional classical MD. This increase in speed is possible because GCMD replaces the most time-consuming part of CMD, i.e., the calculation of the average centroid force, with an analytical integration. This increase in efficiency due to the analytical Gaussian averaging is in many ways similar to the use of Gaussian basis sets in electronic structure calculations. If the size of the system is large, or when it is coupled to another expensive calculation such as an ab initio (AI) calculation,[11] GCMD may be a good choice or at least a good starting point for a more expensive full CMD calculation. As a realistic example, GCMD was applied in the present work to liquid para-hydrogen/ortho-deuterium where full CMD results were available for comparison. This example reveals that GCMD can be a quite good approximate method for systems at low temperature where quantum effects play a significant role. The computational efficiency of GCMD when utilized in AIMD remains to be determined because the analytical force and its derivative do not exist in AIMD and must be also computed numerically.

Acknowledgment. This research was supported by a grant from the National Science Foundation (CHE-0317132). We thank Dr. Seogjoo Jang for many insightful discussions and Tyler Hone for providing his CMD results on diffusion constants and correlation functions for p-H_2 and o-D_2. An allocation of computer time from the Center for High Performance Computing at the University of Utah is gratefully acknowledged.

Appendices

A. Fitting the Silvera−Goldman Force to Gaussian Functions. When GCMD is adopted for liquid para-hydrogen, the Silvera−Goldman potential of eq 38 or its derivative (force) leads to a singularity problem in the Gaussian integration over [−∞,∞]. Approximating it with several Gaussians can circumvent this singularity problem. The Silvera−Goldman force is given from eq 38 by

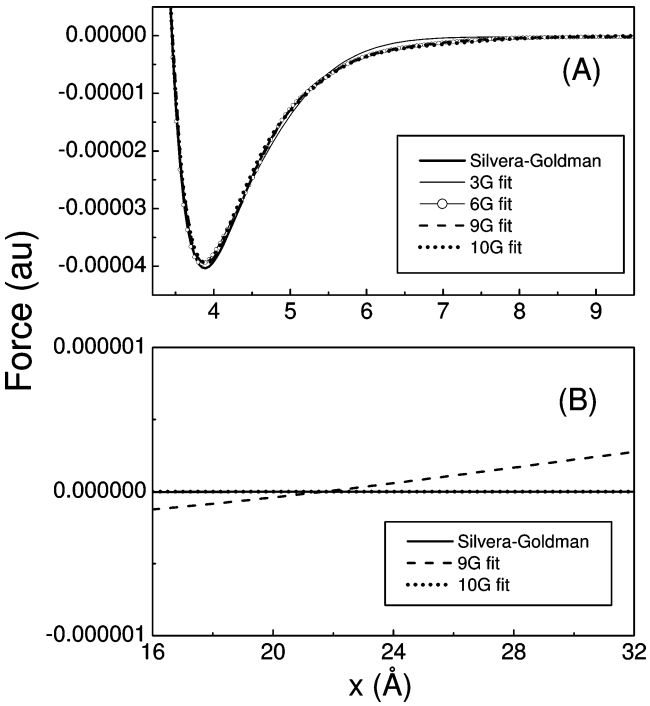

Figure 8. Silvera−Goldman force is fitted to Gaussian function sets. 3-, 6-, 9-, or 10-Gaussians fitted forces are compared. For short-range fitting (A) 9G seems best, whereas a 10G-fitted force describes the best of long-range fitting (B). In the simulations, it is believed that both the equilibrium distance and the long-range part are more important than any other range, so the 10G-fitted force was chosen for this work.

$$F_{SG}(r) = -\frac{d}{dr}V_{SG}(r) = (b + 2cr)\exp[a - br - cr^2] - \left[\frac{6C_6}{r^7} + \frac{8C_8}{r^9} - \frac{9C_9}{r^{10}} + \frac{10C_{10}}{r^{11}}\right]f_c(r) - \left[\frac{C_6}{r^6} + \frac{C_8}{r^8} - \frac{C_9}{r^9} + \frac{C_{10}}{r^{10}}\right]f_c'(r) \quad \text{(A1)}$$

where

$$f_c'(r) = \begin{cases} (2.56r_m/r^2)((1.28r_m/r) - 1)f_c(r), & r < 1.28r_m \\ 0, & r \geq 1.28r_m \end{cases} \quad \text{(A2)}$$

This force can be written as with the superposition of N_G Gaussians as follows.

$$F_{SG}(r) \approx \sum_{n=1}^{N_G}[A_n e^{-2(r-r_n)^2/w_n^2} + B_n] \quad \text{(A3)}$$

A different range of the fitting potential will require a different number of Gaussians. This fitting range should be large enough to cover any significant distributions which are shown in Figure 1S of the Supporting Information. Since the tail of GQDO-0 along the v-direction at 14 K is found in the most inner bound region, this should be taken into account in the determination of the inner bound of the fitting range. As such, an appropriate inner bound of the fitted force should be around 2.1 Å. Figure 8 shows the 9G-fitting (Supporting Information) has the best fit around the minimum force, while Figure 8B suggests 10G-fitting is better for the long-range behavior. Since the average contact range and the long-range are more important in this

simulation, the 10G-fitting within the range [2.1 Å, 52.9 Å] was chosen for this work. This range [2.1 Å, 52.9 Å] guarantees inclusion of most parts of the GQDO over the whole distribution, so that the Gaussian centroid force integrated within this range will have a small error. Also this range sufficiently covers the size of the simulation box (27.9 Å) or the region of the minimum image convention. The parameters for the fitted force with 10 Gaussians is given in the Supporting Information.

B. Gaussian Centroid Force. Once any type of GCMD in section II.C is employed, the Gaussian centroid force of the Silvera−Goldman force has the following form

$$F_G(r_c) = Tr[\hat{\delta}_G \hat{F}] = \int dr F_{SG}(r) \cdot \sqrt{\frac{\gamma_G}{\pi}} e^{-\gamma_G (r-r_c)^2} \quad \text{(B1)}$$

$$F_G(r_c) = \sum_{n=1}^{N_G} [A_n \sqrt{g_n} e^{-2g_n (r_c - r_n)^2 / {w_n}^2} + B_n] \quad \text{(B2)}$$

$$g_n \equiv \frac{\gamma_G}{\gamma_G + 2/{w_n}^2} \quad \text{(B3)}$$

and the value of γ_G depends on the type of GCMD from section II.C.

If a system consists of N_{H_2} hydrogen molecules, each pair of hydrogen molecules experiences this Gaussian centroid force, and there are a total of $N_{H_2}(N_{H_2} - 1)/2$ calculations of the Gaussian centroid force required for each propagation of the whole system. Appendix C describes the Gaussian centroid force in a many-particle system. With that in mind, each hydrogen molecule propagates under the force that is the vector sum of $N_{H_2} - 1$ Gaussian centroid forces from other hydrogen molecules. For a better notation for pairwise interacting systems, the centroid position, r_c in eq B2, is replaced by the distance between the ith hydrogen and the jth hydrogen molecules, r_{ij}. Therefore, the total Gaussian centroid force exerted on the ith hydrogen is expressed as

$$\mathbf{F}_G(\mathbf{r}_i) = \sum_{j=1}^{N_{H_2}-1} \hat{\mathbf{r}}_{ij} \sum_n \left[A_n \sqrt{\frac{\gamma_G}{\gamma_G + 2/{w_n}^2}} e^{-2\gamma_G (r_{ij} - r_n)^2 / {w_n}^2} + B_n \right] \quad \text{(B4)}$$

where $\mathbf{r}_i$ is a position of the ith hydrogen and $\hat{\mathbf{r}}_{ij}$ is a unit vector pointing from the jth hydrogen to the ith hydrogen, i.e. $\hat{\mathbf{r}}_{ij} = (\mathbf{r}_i - \mathbf{r}_j)/r_{ij}$. It should be noted that cross-correlations have been neglected in defining the GCMD width and Gaussian-averaged centroid force in the above equation (see below).

C. Gaussian Centroid Force in Many-Particle System. *1. Pairwise Additivity Assumption of the Gaussian Centroid Force.* For an N-body system, the Gaussian centroid force on the ith particle is, in principle, defined as

$$\mathbf{F}_{i,G}(\mathbf{r}_{i,G}) = \sum_{m=1}^{3} \hat{\mathbf{r}}_{im} \left[\int dr_{im} \left(-\frac{\partial V_i(\mathbf{r}_i)}{\partial r_{im}} \right) \sqrt{\frac{\gamma_{im,G}}{\pi}} e^{-\gamma_{im,G} (r_{im} - r_{im,G})^2} \right] \quad \text{(C1)}$$

where $\mathbf{r}_{i,G}$ and r_{im} are the Gaussian centroid position and the m-direction coordinate (normally x, y, or z) of the ith particle. The $\gamma_{im,G}$ in eq C1 is defined in the same way as in eqs 13 or 16 except that this requires a calculation of the quantity, $\partial^2 V_i(\mathbf{r}_i)/\partial {r_{im}}^2$ for $V_i(\mathbf{r}_i) = \sum_{j=1}^{N-1} V_{ij}(r_{ij})$ where V_{ij} is a pair potential between particle i and particle j. Doing this in many-particle systems is actually very cumbersome so a more practical approach is chosen below. It is helpful, however, to explore aspects of the above approach before delving into the details. For example, each particle in a many-body system is located either at the boundary or inside a cluster as shown in Figure 9. Figure 9 shows spatial arrangements of hydrogen molecules which are used in the calculations of distribution functions in Figure 1S. The potentials exerted on the inside particles along each direction have functional forms as given in the Supporting Information. Note that these potentials and forces are expressed along a single direction (f, e, or υ) rather than in 3-dimensional coordinates. Classical distribution functions ($P = 1$), which are just Boltzman distributions, $\exp[-\beta V(r)]$, are also shown in the same Figure 1S of the Supporting Information for comparison. Centroid distributions come from PIMD using an isomorphic ring polymer.[35] A quantum particle described by a ring polymer of $P = 10$ beads distributes over a little narrower range in comparison to a classical particle. Of course any particle will be inside a cluster if one uses periodic boundary conditions in simulations. From Figure 1S, one can see that both the distribution and QDO are not much different along any direction (f, e, or υ) once a particle is surrounded by other particles, so one can also determine a proper inner bound for the fitted force.

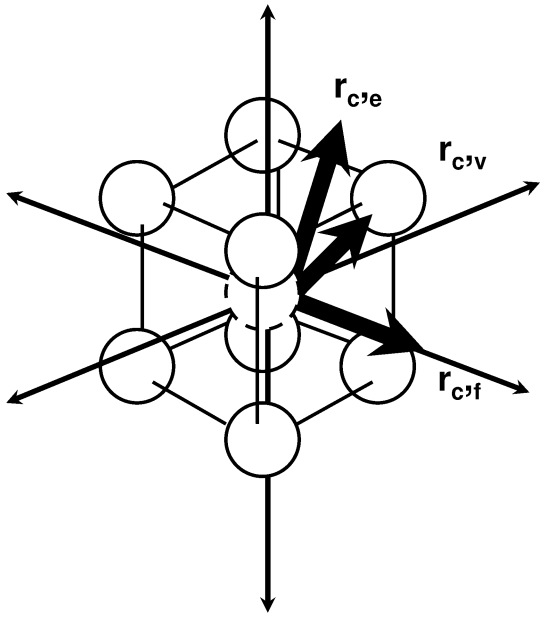

Figure 9. Hydrogen molecules in a body-centered cubic. Thick arrows show directions along which distributions are calculated in Figure 1S of the Supporting Information.

A more practical approach is to calculate a direct Gaussian centroid force for each pair interaction and then do the vector sum for each particle, such that

$$\mathbf{F}_{i,G}(\mathbf{r}_{i,G}) = \sum_{j=1}^{N-1} \hat{\mathbf{r}}_{ij} \left[\int dr_{ij} \left(-\frac{\partial V_{ij}(r_{ij})}{\partial r_{ij}} \right) \sqrt{\frac{\gamma_{ij,G}}{\pi}} e^{-\gamma_{ij,G} (r_{ij} - r_{ij,G})^2} \right] \quad \text{(C2)}$$

This is the "pairwise additivity assumption" of GCMD. In the viewpoint of classical dynamics, it is natural to think of the total force on a particle as the same as a vector sum of forces from all pairs. It is, however, an additional assumption in the GCMD formalism to consider a vector sum of Gaussian forces of the pair interactions, eq C2, instead of eq C1. This assumption not only makes the method more practical but also results in a quite good description which is confirmed in section III.

2. Gaussian Centroid Force for Each Pair-Interaction. Once the pairwise additivity assumption described in the previous section is accepted, another issue still remains because a pair-interaction generally has a singular point at zero distance and its Gaussian average, eq C3, becomes divergent, i.e.

$$F_{ij,G}(r_{ij,G}) = Tr[\hat{\delta}_{ij,G}\hat{F}_{ij}] = \int dr_{ij}\left(-\frac{\partial V_{ij}(r_{ij})}{\partial r_{ij}}\right)\sqrt{\frac{\gamma_{ij,G}}{\pi}}e^{-\gamma_{ij,G}(r_{ij}-r_{ij,G})^2} \quad \text{(C3)}$$

There are two possible ways to circumvent this problem. One is using a tapered force at the singular point, cutting the Gaussian tail at the proper range, and then integrating eq C3 numerically. The other one is fitting the pair-interaction within the relevant range into a superposition of several Gaussian functions.

As stated in the main text, the second method is usually superior in computational efficiency to the first method mainly by virtue of the analytic integration in eq C3 for a Gaussian-fitted force. In the case that fitting the pair-interaction into a superposition of Gaussians is difficult, the first method could be a more effective choice. The current work on para-hydrogen/ortho-deuterium uses the second method to get a Gaussian centroid force for the pair-interaction, the details of which are given in Appendices A and B.

Supporting Information Available: Gaussian functions set used in fitting Silvera−Goldman force, the potential exerted on an inside particle of a cluster, and its corresponding distribution functions and QDOs. This material is available free of charge via the Internet at http://pubs.acs.org.

References and Notes

(1) Cao, J.; Voth, G. A. *J. Chem. Phys.* **1993**, *99*, 10070.
(2) Cao, J.; Voth, G. A. *J. Chem. Phys.* **1994**, *100*, 5093.
(3) Cao, J.; Voth, G. A. *J. Chem. Phys.* **1994**, *100*, 5106.
(4) Cao, J.; Voth, G. A. *J. Chem. Phys.* **1994**, *101*, 6157.
(5) Cao, J.; Voth, G. A. *J. Chem. Phys.* **1994**, *101*, 6168.
(6) Jang, S.; Voth, G. A. *J. Chem. Phys.* **1999**, *111*, 2357.
(7) Jang, S.; Voth, G. A. *J. Chem. Phys.* **1999**, *111*, 2371.
(8) D. Thirumalai, E. J. Bruskin, B. J. Berne, *J. Chem. Phys.* **1983**, *79*, 5063.
(9) Schmitt, U. W.; Voth, G. A. *J. Chem. Phys.* **1999**, *111*, 9361.
(10) Kim, J.; Schmitt, U. W.; Gruetzmacher, J. A.; Voth, G. A.; Scherer, N. F. *J. Chem. Phys.* **2002**, *116*, 737−746.
(11) Pavese, M.; Voth, G. A. *Chem. Phys. Lett.* **1996**, *249*, 231.
(12) Kinugawa, K. *Chem. Phys. Lett.* **1998**, *292*, 454.
(13) Bermejo, F. J.; Kinugawa, K.; Cabrillo, C.; Bennington, S. M.; Fak, B.; Fernandez-Diaz, M. T.; Verkerk, P.; Dawidowski, J.; Fernandez-Perea, R. *Phys. Rev. Lett.* **2000**, *84*, 5359.
(14) Calhoun, A.; Pavese, M.; Voth, G. A. *Chem. Phys. Lett.* **1996**, *262*, 415.
(15) Yonetani, Y.; Kinugawa, K. *J. Chem. Phys.* **2003**, *119*, 9651.
(16) Saito, H.; Nagao, H.; Nishikawa, K.; Kinugawa, K. *J. Chem. Phys.* **2003**, *119*, 953.
(17) Hone, T. D.; Voth, G. A. *J. Chem. Phys.* **2004**, *121*, 6412.
(18) Miura, S.; Okazaki, S.; Kinugawa, K. *J. Chem. Phys.* **1999**, *110*, 4523.
(19) Poulsen, J.; Rossky, P. J. *J. Chem. Phys.* **2001**, *115*, 8014.
(20) Poulsen, J.; Rossky, P. J. *J. Chem. Phys.* **2001**, *115*, 8024.
(21) Poulsen, J.; Keiding, S. R.; Rossky, P. J. *Chem. Phys. Lett.* **2001**, *336*, 488.
(22) Shi, Q.; Geva, E. *J. Chem. Phys.* **2003**, *119*, 9030.
(23) Schenter, G. K.; Garrett, B. C.; Voth, G. A. *J. Chem. Phys.* **2000**, *113*, 5171.
(24) Marx, D.; Tuckerman, M. E.; Martyna, G. J. *Comput. Phys. Comm.* **1999**, *118*, 166.
(25) Jang, S.; Voth, G. A. *J. Chem. Phys.* **2000**, *112*, 8747.
(26) Geva, E.; Shi, Q.; Voth, G. A. *J. Chem. Phys.* **2001**, *115*, 9209.
(27) Schenter, G. K.; Messina, M.; Garrett, B. C. *J. Chem. Phys.* **1993**, *99*, 1674.
(28) Pavese, M.; Berard, D. R.; Voth, G. A. *Chem. Phys. Lett.* **1999**, *300*, 93.
(29) Hone, T. D.; Izvekov, S.; D. R.; Voth, G. A. *J. Chem. Phys.* **2005**, *122*, 054105(1−7).
(30) Martyna, G. J.; Klein, M. L.; Tuckerman, M. *J. Chem. Phys.* **1992**, *97*, 2635.
(31) Jang, S.; Voth, G. A. *J. Chem. Phys.* **1997**, *107*, 9514.
(32) Ka, B. J.; Voth, G. A. *J. Phys. Chem. B* **2004**, *108*, 6883.
(33) Sun, X.; Miller, W. H. *J. Chem. Phys.* **1999**, *110*, 6635.
(34) Silvera, I. F.; Goldman, V. V. *J. Chem. Phys.* **1978**, *69*, 4209.
(35) An initial ring-polymer was built at the position of classical distribution ($r = 6.59506$ au at $T = 14$K) with a radius of 0.5 au and then relaxed 1,000,000 steps with a time step of 0.01, and then centroid positions at every 10,000 steps were collected till the total number of r_c is 10,000.
(36) Jang, S.; Voth, G. A. *J. Chem. Phys.* **1998**, *107*, 4098.
(37) Esel'son, B. N.; Blagoi, Y. P.; Grigor'ev, V. V.; Manzhelii, V. G.; Mikhailenko, S. A.; Neklyudov, N. P. *Properties of Liquid and Solid Hydrogen*; Israel Program for Scientific Translations: Jerusalem, 1971.
(38) Mukherjee, M.; Bermejo, F. J.; Fak, B.; Bennington, S. M. *Europhys. Lett.* **1997**, *40*, 153.